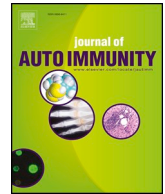




Since January 2020 Elsevier has created a COVID-19 resource centre with free information in English and Mandarin on the novel coronavirus COVID-19. The COVID-19 resource centre is hosted on Elsevier Connect, the company's public news and information website.

Elsevier hereby grants permission to make all its COVID-19-related research that is available on the COVID-19 resource centre - including this research content - immediately available in PubMed Central and other publicly funded repositories, such as the WHO COVID database with rights for unrestricted research re-use and analyses in any form or by any means with acknowledgement of the original source. These permissions are granted for free by Elsevier for as long as the COVID-19 resource centre remains active.



Prostaglandin D2 signaling in dendritic cells is critical for the development of EAE

Jian Zheng^a, Alan Sariol^b, David Meyerholz^c, Qinran Zhang^d, Juan E. Abrahante Lloréns^e, Shuh Narumiya^f, Stanley Perlman^{a,b,*}

^a Department of Microbiology and Immunology, University of Iowa, Iowa City, IA, USA

^b Interdisciplinary Program in Immunology, University of Iowa, Iowa City, IA, USA

^c Department of Pathology, University of Iowa, Iowa City, IA, USA

^d School of Mathematics and Statistics, Wuhan University, Wuhan, PR China

^e University of Minnesota Informatics Institute (UMII), Minneapolis, MN, USA

^f Department of Pharmacology, Kyoto University, Tokyo, 606-8501, Japan

ARTICLE INFO

Keywords:

EAE
Prostaglandin D2
PTGDR
DCs
IL-1 β

ABSTRACT

Priming of autoreactive T cells in lymph nodes by dendritic cells (DCs) is critical for the pathogenesis of experimental autoimmune encephalitis (EAE). DC activation reflects a balance of pro- and anti-inflammatory signals. One anti-inflammatory factor is prostaglandin D2 signaling through its cognate receptor, D-prostanoid receptor 1 (PTGDR), on myeloid cells. Loss of PTGDR signaling might be expected to enhance DC activation and EAE but here we show that PTGDR^{-/-} mice developed only mild signs of MOG₃₅₋₅₅ peptide immunization-induced EAE. Compared to wild type mice, PTGDR^{-/-} mice exhibited less demyelination, decreased leukocyte infiltration and diminished microglia activation. These effects resulted from increased pro-inflammatory responses in the lymph nodes, most notably in IL-1 β production, with the unexpected consequence of increased activation-induced apoptosis of MOG₃₅₋₅₅ peptide-specific T cells. Conditional deletion of PTGDR on DCs, and not other myeloid cells ameliorated EAE. Together, these results demonstrate the indispensable role that PGD₂/PTGDR signaling on DCs has in development of pathogenic T cells in autoimmune demyelination.

1. Introduction

Multiple sclerosis (MS), the most common human demyelinating disease, has environmental, genetic and immune components [1–4]. Most of the clinical and pathological manifestations result from the effects of autoreactive T cells or antibodies. Experimental autoimmune encephalomyelitis (EAE), a commonly used model for MS, is generally induced by peripheral immunization with an autoantigen, such as myelin oligodendrocyte glycoprotein (MOG) or a MOG-specific peptide (MOG₃₅₋₅₅, spanning residues 35–55). EAE is triggered by breakdown of the blood-brain barrier (BBB), which facilitates the infiltration of peripheral autoreactive lymphocytes. Pathogenic IFN- γ - and IL-17-secreting CD4 T cells, or CD8 T cells or, in some settings, B cells, represent the major contributors to the pathophysiology of MS and EAE [5–8]. A key step in the generation of autoreactive (anti-myelin) T cells is priming by antigen presenting cells (APCs), especially dendritic cells (DCs), in lymph nodes (LNs).

DC activation and subsequent T cell priming are multi-faceted with

involvement of the T cell receptor and co-stimulatory and other molecules [9–11]. Myeloid cells also express cytokines and chemokines that contribute to EAE pathogenesis [12–14]. We recently identified a role for prostaglandin D2 (PGD₂) signaling in DC activation in the brain and lung in the context of coronavirus infection [15,16]. PGD₂, the most abundantly expressed prostaglandin in the brain [17], has both anti-inflammatory and pro-inflammatory properties, depending on whether it binds to the PTGDR (D-prostanoid 1 receptor, DP1) on myeloid cells like Langerhans cells and DCs [18–21] or to the DP2/CRTH2 receptor on Th2 CD4 T cells [22]. Of note, DP1 is also expressed on other hematopoietic and non-hematopoietic cells such as eosinophils, neurons and astrocytes [23–26]. PGD₂/PTGDR signaling triggers G protein activation and cAMP production and plays a role in neuroprotection after ischemia, astrogliosis and demyelination in twitcher mice, as well as in spinal cord contusion injury [27–32]. In addition, PGD₂/PTGDR signaling also regulates the sleep–wake cycle [32].

PGD₂/PTGDR signaling is necessary for diminishing autoimmune arthritis in mice [21] and for optimal microglia/macrophage activation

* Corresponding author. Department of Microbiology and Immunology, University of Iowa, Iowa city, IA, USA.

E-mail address: stanley-perlman@uiowa.edu (S. Perlman).

<https://doi.org/10.1016/j.jaut.2020.102508>

Received 14 May 2020; Received in revised form 8 June 2020; Accepted 12 June 2020

Available online 02 July 2020

0896-8411/ © 2020 Elsevier Ltd. All rights reserved.

and IFN expression after infection with a neurotropic coronavirus (mouse hepatitis virus, MHV). MHV causes acute encephalitis and acute and chronic demyelinating encephalomyelitis. In the absence of PTGDR signaling (mice genetically deficient in PTGDR expression (PTGDR^{-/-} mice, called “PTGDR^{-/-}” herein), the innate immune response was dysregulated, with delayed IFN-I production and increased inflammatory activation compared to B6 mice. IL-1 β expression was increased in PTGDR^{-/-} mice and resulted in increased mortality, which could be reversed by treatment with Anakinra, an IL-1 β R blocker. Since IL-1 β is known to exacerbate EAE as well as MS [13,33] and inflammatory activation is increased in PTGDR^{-/-} mice, we reasoned that PTGDR^{-/-} mice would develop more severe EAE than B6 mice.

However, in contrast to this expectation, PTGDR^{-/-} mice were protected from severe MOG₃₅₋₅₅ peptide-induced EAE, and developed milder clinical disease and less demyelination compared to B6 mice. Here, we focused on myeloid cell function, recognizing that other cells also express PTGDR [23–26]. We found that the absence of PTGDR expression on dendritic cells resulted in increased apoptosis of activated myelin-specific T cells in peripheral lymphoid tissues and reduced numbers of CNS-infiltrating pathogenic T cells. We also showed that similar processes occurred in human cells, identifying a potential target for preventing the initiation or relapse of CNS autoimmune disease.

2. Material and methods

2.1. Mice

B6-129P2-Cx3cr1^{tm2.1(cre/ERT2)}Litt/WganJ (“CX3CR1-Cre”), B6-129P2-Lyz2^{tm1(cre)lfo}/J (“LysM-Cre”) and B6. Cg-Zbtb46^{tm3.1(cre)Mnz}/J (“zDC-Cre”) (all on a C57BL/6 J background) were purchased from Jackson Laboratories. PTGDR^{-/-} mice were generated as described previously [34] and were obtained from the Department of Pharmacology, Kyoto University, Tokyo, Japan, along with control mice (B6, C57BL/6 J background) [34]. PTGDR^{fllox} (C57BL/6 J background) mice were obtained from Dr. Richard Breyer, Vanderbilt University. In this study, CX3CR1-Cre, LysM-Cre and zDC-Cre mice were crossed to PTGDR^{fllox} mice to generate CX3CR1-, LysM- and zDC-conditional PTGDR knock-out mice (CX3CR1-PTGDR^{-/-}, LysM-PTGDR^{-/-} and zDC-PTGDR^{-/-} mice) respectively. To induce Cre production, 3wk CX3CR1-conditional PTGDR knock-out and corresponding control mice were all treated with 2 doses of tamoxifen (10mg/dose) at 0 and 48 h via oral gavage (p.o.) and then rested for 4 weeks before immunization to reduce tamoxifen-caused effects. All animal studies were approved by the University of Iowa Animal Care and Use Committee and met stipulations of the Guide for the Care and Use of Laboratory Animals.

2.2. Generation of EAE

Before the induction of EAE, all mice were kept in the same environment for at least 10 days to reduce microbiome differences. For MOG₃₅₋₅₅ peptide immunization, mice were lightly anesthetized with isoflurane and subcutaneously (s.c.) immunized with 0.2 mg MOG₃₅₋₅₅ peptide (MEVGWYRSPFSRVVHLYRNGK, Bio-synthesis) in 0.1 ml PBS plus 0.1 ml complete Freund's adjuvant (CFA) (Thermo-Fisher) supplemented with 0.4 mg *M. tuberculosis* H37 Ra (BD). On day 0 and 2 post immunization, mice were intravenously (i.v.) injected with 0.2 μ g Pertussis toxin (List Biological Laboratories) in 0.2 ml PBS. Treated mice were monitored daily and the disease score was determined as follows: 0: no clinical sign, 1: weakness of the tail, 2: complete tail paralysis, 3: partial hind limb paralysis, 4: complete hind limb paralysis, 5: incontinence and partial or complete paralysis of forelimbs, 6: death [35].

2.3. Histology

Animals were anesthetized and transcardially perfused with PBS

followed by zinc formalin. Brains, spinal cords, and LNs (axillary, brachial and inguinal) were removed, fixed in zinc formalin, and paraffin embedded. Sections were stained with hematoxylin and eosin. Alternatively, fixed spinal cord sections were deparaffinized and hydrated with 95% EtOH, followed by staining with Luxol Fast Blue solution at 56°C–58°C overnight. Stained sections were then washed with 95% EtOH and H₂O before differentiation with lithium carbonate and 70% EtOH. Images were acquired using a BX61 light microscope (Olympus) and CellSens software (Olympus). The percentage of demyelination (% demyelinated/total white matter of the spinal cord) was determined using ImageJ 64 (NIH) software.

2.4. Confocal microscopy

Tissues were harvested as described above and fixed with 4% PFA at 4°C for 4 h, followed by immersion in 10%, 20%, 30% sucrose-PBS for 12 h each. 5–15 μ m thick sections were then prepared from OTC-embedded samples and fixed in acetone for 10 min at 4°C. For staining, sections were blocked with goat serum for 2 h at room temperature (RT) and treated with primary antibodies (rat anti-mouse CD3 (CD3-12), hamster anti-mouse CD11c (N418), rabbit anti-mouse cleaved caspase 3 (Abcam)) prior to incubation overnight at 4°C. After washing with PBS, samples were exposed to secondary antibodies (Alexa 647-goat anti-rabbit IgG, Alexa 488-goat anti-hamster IgG, Alexa 568-goat anti-rat IgG, Abcam) for 30 min. Finally, slides were overlaid with DAPI (Vector) and examined with a confocal microscope (Zeiss 710).

2.5. Antibodies and flow cytometry

The following monoclonal antibodies were used: PE or PerCP-Cy5.5-conjugated rat anti-mouse CD4 (RM4-5), FITC-conjugated rat anti-mouse CD8 (53–6.7), FITC or e450-conjugated hamster anti-mouse CD11c (HL3), PerCP-Cy5.5-conjugated mouse anti-mouse Ly-6C (HK1.4), APC-conjugated rat anti-mouse F4/80 (BM8), FITC-conjugated rat anti-mouse IL-1 β (NJTEN3), PerCP-Cy5.5-conjugated mouse anti-mouse Foxp3 (FJK-16s) and rat anti-mouse CD16/32 (2.4G2) (eBioScience); PerCP-Cy5.5-conjugated mouse anti-human CD4 (RPA-T4), PerCP-Cy5.5-conjugated hamster anti-mouse CD3 (145-2C11), Brilliant Violet 421-conjugated mouse anti-mouse CD45.1 (A20), APC-conjugated mouse anti-mouse CD45.2 (104), PE-Cy7-conjugated mouse anti-mouse NK1.1 (PK-136), PerCP-Cy5.5 or PE-conjugated rat anti-mouse CD45 (30-F11), APC-Cy7-conjugated mouse anti-mouse MHC-I (28-8-6), Brilliant Violet 510-conjugated mouse anti-mouse MHC-II (M5/114.15.2), PE-conjugated mouse anti-mouse CD80 (2D10), PE-Cy7-conjugated mouse anti-mouse CD83 (HB15e), PE-Cy7-conjugated mouse anti-mouse PD-1 (RPM1-30), PE-conjugated mouse anti-mouse Fas (SA367H8), APC/Fire 750-conjugated goat anti-rat IgG (poly4054), Alexa Fluor 488-conjugated rat anti-mouse IL-2 (JES6-5H4), APC-conjugated rat anti-mouse IL-6 (MP5-20F3), Alexa Fluor 647-conjugated rat anti-mouse IL-10 (JES5-16E3), PE-conjugated rat anti-mouse IL-12 (C15.6), Alexa Fluor 647 or APC-conjugated rat anti-mouse IFN- γ (XMG1.2), PE-conjugated mouse anti-mouse IL-17F (9D3.1C8), APC-conjugated rat anti-mouse IL-17A (TC11-18H10.1) and APC-conjugated rat anti-mouse TNF (MP6-XT22) (BioLegend); rat anti-mouse CXCR5 (2G8), FITC-conjugated mouse anti-mouse B220 (RA3-6B2), PE-conjugated rat anti-mouse Ly-6G (1A8), FITC-conjugated rabbit anti-mouse caspase-3 (C92-605), FITC-conjugated rat anti-mouse CD86 (GL1) (BD); rabbit anti-mouse cleaved caspase 3 (Abcam); PE-conjugated rat anti-mouse CCR2 (475,301) (R&D).

For surface staining, 10⁶ cells were blocked with 1 μ g of anti-CD16/32 antibody and stained with the indicated antibodies at 4°C. For CXCR5 staining, cells were treated with unconjugated anti-CXCR5 antibody at 37°C for 1 h followed by secondary antibody at RT for 30 min. For intracellular staining, cells were fixed using Cytofix Solution (BD) and stained for Foxp3 or intracellular cytokines. To detect antigen-specific T cells, 10⁶ cells were cultured in a 96-well round bottom plate

in the presence of Brefeldin A (BFA, Invitrogen) and MOG₃₅₋₅₅ peptide (Bio-Synthesis) for 6–12 h. To determine the absolute number of cells, CountBright™ absolute counting beads (Invitrogen) were added during staining. A Dead Cell Apoptosis Kit with Annexin V FITC and PI (Thermo Fisher) was used to gate live cells. Flow cytometric data were acquired using a FACSVerser (BD) and were analyzed using FlowJo software (Tree Star).

2.6. CD11c⁺ cell separation using magnetic beads and adoptive transfer

Spleen single-cell suspensions were prepared as described. CD11c⁺ cells were obtained from spleens of unimmunized Flt3-treated B6 or PTGDR^{-/-} mice [36] using anti-mouse CD11c MicroBeads (Miltenyi Biotec) with an autoMACS system (Miltenyi Biotec) following the manufacturer's protocol. In some experiments, 10⁶ CD11c⁺ cells were loaded with MOG₃₅₋₅₅ peptide and adoptively transferred i. v. into B6 or PTGDR^{-/-} mice at the indicated time points.

2.7. Evans blue permeability assay

4–6wk wild type or PTGDR^{-/-} mice were injected with 0.2 µg Pertussis toxin (List Biological Laboratories) in 0.2 ml PBS i. v. on day 0 and 2. Evans blue (EB) (2%, 2 ml/kg) was then injected i. v. at 0.5 h before perfusion. Brains were removed, weighed and homogenized in 0.75 ml of PBS and 0.25 ml of 100% TCA solution before cooling overnight at 4 °C. Samples were then centrifuged for 30 min at 1000 × g at 4 °C. EB in the supernatants of each sample was subsequently quantified using a 96-well plate reader. All measurements were within the range of detection established by a standard curve.

2.8. BrdU staining and analysis

To detect proliferating cells, 0.8 mg/ml BrdU (BD Bioscience) was added to the drinking water for 10 days before immunization and analyzed by flow cytometry.

2.9. Adoptive transfer of T lymphocytes

Single cell suspensions were prepared from spleen of wild type or PTGDR^{-/-} mice and then cultured in 10% FBS-RPMI (Gibco) at 4 × 10⁶ cells/ml, supplemented with 5 µg/ml MOG₃₅₋₅₅ peptide, 10 ng/ml mouse IL-1α, 5 ng/ml mouse IL-23 (Peprotech), and 10 µg/ml anti-mouse IFN-γ (XMG1.2, eBioscience) to induce the outgrowth of Th17 cells [37]. 96 h later, CD4 T cells were purified using a CD4⁺ T Cell Isolation Kit II, Mouse (Miltenyi) and 40 × 10⁶ cells/mouse were injected intraperitoneally (i.p.) into recipient mice. Donor T cells were tracked by staining with 1 mM CFSE (Thermo Fisher) for 15 min at 37 °C before adoptive transfer.

2.10. PD-1/PD-L1, Fas/FasL and IL-1β blockade

For *in vitro* blockade, hamster anti-mouse PD-1 antibody (J43) or hamster anti-mouse FasL antibody (MFL3, BioXCell) was added at a final concentration of 10 µg/ml at the start of culture. For *in vivo* blockade, hamster anti-mouse PD-1 antibody (J43, 10 µg/g weight), hamster anti-mouse FasL antibody (MFL3, 10 µg/g weight) or Anakinra (2 µg/g weight, Amgen) was injected i. p. at the indicated timepoints.

2.11. CD4 and CD8 T cell depletion

4–6wk mice were injected with anti-mouse CD4 (clone GK1.5, 250µg/mouse) or CD8 antibody (clone 2.43 250µg/mouse, Bio X Cell) i. v. on day -2, 0 and 2 post immunization to deplete CD4 or CD8 T cells, respectively.

2.12. Next generation sequencing (NextSeq)

RNA from CD11c⁺ cells from LNs (axillary, brachial and inguinal) of immunized mice was purified using a mirVana kit (Life Technologies) according to the manufacturer's instructions and processed and analyzed at the University of Minnesota Genomics Facility. Briefly, truSeq libraries (Illumina) were hybridized to a NextSeq (single read, Illumina). After being quantified using a fluorimetric RiboGreen assay, samples were then converted to Illumina sequencing libraries.

Library Creation: Total RNA samples were converted to Takara sequencing libraries using Takara Bio's SMARTer Stranded Total RNA-Seq – Pico Mammalian Kit v2 (Cat. # 634,414). In summary, between 250 pg and 10ng of total RNA was fragmented and then reverse transcribed into cDNA using random primers. The Template Switching Oligo (TSO) was incorporated during cDNA synthesis and allowed for full length cDNA synthesis and strand specificity to be retained. Illumina sequencing adapters and barcodes were then added to the cDNA via limited PCR amplification. Next, mammalian ribosomal cDNA was enzymatically cleaved. Uncleaved fragments are PCR enriched 12–16 cycles. Final library size distribution was validated using capillary electrophoresis and quantified using fluorimetry (PicoGreen). Indexed libraries were then normalized and pooled for sequencing.

Cluster generation and sequencing: Pooled libraries were denatured and diluted to the appropriate clustering concentration (1.5pM for Mid-output and 1.8pM for High-output). Denatured and diluted libraries were loaded onto the NextSeq 550 cartridge and clustering occurs on-board the instrument. Once clustering was complete, sequencing immediately commenced using Illumina's 2-color SBS chemistry. Upon completion of read 1, an index read 1 of varying length is performed depending on the library kit used. Libraries were dual indexed, so a second index read was performed. Finally, the library fragments were re-synthesized in reverse orientation and sequenced from the opposite end of the read 1 fragment to produce the paired end read 2.

Primary analysis and de-multiplexing: Base call (.bcl) files for each cycle of sequencing were generated by Illumina Real Time Analysis [38] software. The base call files and run folders were then exported to servers maintained at the Minnesota Supercomputing Institute. Primary analysis and de-multiplexing were performed using Illumina's CASAVA software 1.8.2. The end result of the CASAVA workflow is de-multiplexed FASTQ files that were released for subsequent analysis.

Further analysis: 75 FastQ single reads (n = 23.6 million average per sample) were trimmed using Trimmomatic (v 0.33) enabled with the optional “-q” option; 3bp sliding-window trimming from 3' end requiring minimum Q30. Quality control on raw sequence data for each sample was performed with FastQC. Read mapping was performed via Hisat2 (v2.1.0) using the mouse genome (mm10) as reference. Gene quantification was done via Feature Counts for raw read counts. Differentially expressed genes were identified using the edgeR (negative binomial) feature in CLCGWB (Qiagen, Redwood city, CA) using raw read counts. We filtered the generated list based on a minimum 2X Absolute Fold Change and FDR corrected p < 0.05. These filtered genes were then imported into Ingenuity Pathway Analysis Software (Qiagen, Redwood city, CA) for pathway identification. Complete RNA-Seq data were deposited in the NCBI's Gene Expression Omnibus (GEO) database (GSE71868).

2.13. CRISPR-Cas9 editing

Human MDDCs were treated with PTGDR plasmid (sc-422478-HDR) or control plasmid as per manufacturer's instructions (Santa Cruz Biotechnology, Inc). Briefly, cells were plated at 2 × 10⁶ in 3 ml antibiotic-free RP-10 per well in 6-well plate, 24 h before transfection. For each transfection, 1.5 µg of plasmid DNA was diluted with transfection medium to bring the final volume to 150 µl and mixed with transfection reagent prior to dropwise addition to cells. Cells were incubated for 72–96 h. The efficacy of editing was determined by PCR. Cells were

stimulated with LPS for 16 h. Total RNA was extracted from human MDDCs using TRIzol reagent (Invitrogen) and used for RT-PCR analysis as previously described [39]. Cycle threshold values were normalized to those of the housekeeping gene hypoxanthine phosphoribosyl-transferase (HPRT) by the following equation: $D_{Ct} = C_{t(\text{gene of interest})} - C_{t(\text{HPRT})}$. All results are shown as a ratio to HPRT calculated as $2^{-C_{t(\text{gene of interest})}}$.

Primers: mouse PTGDR: F: TCGGTCTTTTATGTGCTCGTG, R: GGATCATCTGGATGA AACACC; human IL-1 β : F: TGGAGAGTGTGGATCCCAAGCAAT, R: TGGAGAGTGTG GATCCCAAGCAAT; human IL-6: F: CTGCAAGAGACTTCCATCCAGTT, R: AAGTAGGG AAGG CCGTGGTT; human IL-10: F: ATAAGTGCACCCACTTCCCA, R: TGGACCATCT TCAC TACGGG; human IL-12: F: ACCACTCCAAAACCTGC, R: CCAGGCAAC TCCCATT AG; human TNF: F: TCGTAGCAAACCACCAAGTG, R: CCTTGAAGAGAACCTGGGAGT; human PTGDR: F: GAAGTTCGTGCAGTACTGTCCAG, R: TCCACTATGGAAATCACA GAC; HGPRT: F: G CGTCGTGATAGCGATGATG, R: CTCGAGCAAGTCTTTCAGTCC.

2.14. Statistics

A Student's *t*-test was used to analyze differences in mean values between groups except in the case of the NGS data. Multiple regression analysis was used to assess differences in weight changes or disease score between different groups adjusted for time after infection. All results are expressed as mean \pm SEM. P-values of < 0.05 were considered statistically significant. *, $P < 0.05$, **, $P < 0.01$. Differences in mortality were analyzed using Kaplan-Meier log-rank survival tests.

3. Results

3.1. PTGDR^{-/-} mice exhibit mild signs of EAE

To assess the role of PGD₂/PTGDR signaling in EAE, 4–6wk PTGDR^{-/-} and wild type mice (B6) were immunized with MOG₃₅₋₅₅ peptide and treated with pertussis toxin as described in Methods (Fig. 1A). B6 mice developed disease at day 10 post-immunization, characterized initially by tail weakness and weight loss, followed by hindlimb and forelimb paralysis (Fig. 1B and C). Approximately 20–40% of B6 mice died by day 30 post-immunization (Fig. 1D), with persistent paralysis in the survivors. In marked contrast, although the incidence of EAE was 100% in PTGDR^{-/-} mice, signs were limited to the tail (paresis or paralysis, scoring 1–2 as described in Methods), and were much milder compared to B6 mice (Fig. 1B). Noteworthy, approximately 30% of PTGDR^{-/-} mice obtained disease-free remission (Supplementary Figure 1A). Histological examination revealed greater demyelination in B6 compared to PTGDR^{-/-} spinal cords (Fig. 1E and F) and no typical pathological changes were observed in B6 and PTGDR^{-/-} brains except minor accumulation of lymphocytes around the ventricles (Supplementary Figure 1B). Consistently, flow cytometric analyses demonstrated higher microglia activation as shown by elevated Iba-1 expression and increased myeloid and/or lymphoid cell infiltration in spinal cords of B6 compared to PTGDR^{-/-} mice (Fig. 1G). Moreover, almost complete remyelination was found in spinal cords of PTGDR^{-/-} mice at day 40 post immunization (Supplementary Figure 1C). Taken together, these results indicate that PTGDR deficiency leads to less severe EAE, characterized by decreased leukocyte infiltration, microglia activation, and demyelination.

3.2. Decreased numbers of MOG₃₅₋₅₅-specific CD4 T lymphocytes in PTGDR^{-/-} mice

MOG₃₅₋₅₅-induced EAE in B6 mice is a CD4 T cell-driven disease [1]. Consistent with this, depletion of CD4 but not CD8 T cells completely protected PTGDR^{-/-} and B6 mice from EAE (Supplementary Fig. 2A and B). To assess the dynamics and functionality of MOG₃₅₋₅₅-specific T cells, CNS and lymphoid tissue (axillary, brachial and inguinal LNs) were harvested and stimulated directly *ex vivo* with peptide. Fewer total

CD3, CD4 and CD8 T cells were identified in LNs and CNS (pooled brain and spinal cord) of immunized PTGDR^{-/-} mice compared to B6 mice when analyzed at different time points (Fig. 2A). Numbers but not percentage of MOG₃₅₋₅₅-specific CD4 T cells (determined by IL-2, IFN- γ , IL-17A and IL-17F expression after *in vitro* stimulation with MOG₃₅₋₅₅ peptide) in the LN were significantly decreased in PTGDR^{-/-} compared to B6 mice at day 10 after immunization (Fig. 2B) whereas equal numbers and percentage of MOG₃₅₋₅₅-specific CD4 T cells (IFN- γ , IL-17A and IL-17F expressing-CD4 T cells after *in vitro* stimulation with MOG₃₅₋₅₅ peptide) were detected in the CNS (Fig. 2C and D). Together, these results suggest that a decreased number of CD4 T cells in the LNs, rather than impairments in expression cytokines or trafficking, contributed to EAE attenuation in PTGDR^{-/-} mice. There were comparable percentages of regulatory T cells (Treg, Foxp3⁺ CD4 T cell) and follicular helper T cells (Tfh, CXCR5⁺PD-1⁺ CD4 T cell) in LNs (Supplementary Figure 2C). Moreover, using an Evans blue assay, we found that blood-brain barrier (BBB) permeability was similar in PTGDR^{-/-} and B6 mice (Fig. 2E and F), suggesting that decreased CNS-infiltrating lymphocytes in PTGDR^{-/-} mice resulted from impaired peripheral expansion or survival, rather than differences in CNS entry.

3.3. Increased activation-induced apoptosis of T cells in LN of PTGDR^{-/-} mice

Since PGD₂/PTGDR signaling is considered anti-inflammatory [18–21], we considered the possibility that CD4 T cell activation was increased in PTGDR^{-/-} mice at times earlier than 10 days after immunization, with subsequent enhanced rates of apoptotic cell death, to explain the results described above. To investigate this possibility, we determined the absolute number of CD4 and CD8 T cells in LNs at days 0, 5 and 10 post immunization by flow cytometry. To reduce the migration of activated T cells to the CNS, pertussis toxin was not administered to mice. On day 5 post-immunization, PTGDR^{-/-} compared to B6 LNs were larger (Supplementary Figure 3A), indicative of increased inflammation, and PTGDR^{-/-} mice contained more CD4 and CD8 T cells in LNs compared to controls (Fig. 3A). In contrast, lymph node size and T cell numbers were decreased by day 10 in PTGDR^{-/-} compared to B6 mice (Fig. 3A, Supplementary Figure 3A). These changes resulted from enhanced apoptosis of CD4 and CD8 T cells harvested from LNs of PTGDR^{-/-} mice on days 10 and 15 as assessed by measurement of caspase-3 (Fig. 3B and C) and increased cell death as assessed by propidium iodide (PI) staining (Supplementary Figure 3B). Moreover, IL-17, and to a lesser extent, IFN- γ -expressing CD4 T cells in the LN of PTGDR^{-/-} mice harvested on day 5 post immunization exhibited a pro-apoptotic phenotype as assessed by annexin-V and PI staining (Supplementary Fig. 3C and D). Additionally, while numbers of CD4 T cells were decreased in the brains and spinal cords of PTGDR^{-/-} compared to wild type mice, the proportion of cells expressing caspase-3 showed no differences (Supplementary Figure 3E), which suggested that the apoptosis of CD4 T cells was limited to LNs. Moreover, the expression of KLRG1, a marker of T cell terminal differentiation, was increased in LN CD4 T cells of PTGDR^{-/-} compared to B6 mice. LN CD4 and CD8 T cell proliferation, as assessed by BrdU incorporation, was lower in PTGDR^{-/-} compared to B6 mice on days 10 and 15 post immunization (Fig. 3D). Taken together, these data suggested that activation-induced apoptosis of CD4 T cells in LNs resulted in decreased numbers of LN and CNS T cells in PTGDR^{-/-} mice, and hence, milder EAE.

3.4. Adoptive transfer of wild type T cells failed to reverse EAE attenuation in PTGDR^{-/-} mice

Diminished number of T cells in the CNS of PTGDR^{-/-} mice could reflect a T cell-intrinsic or T cell-extrinsic defect. To address whether there was a T cell-intrinsic defect, we transferred MOG₃₅₋₅₅-specific

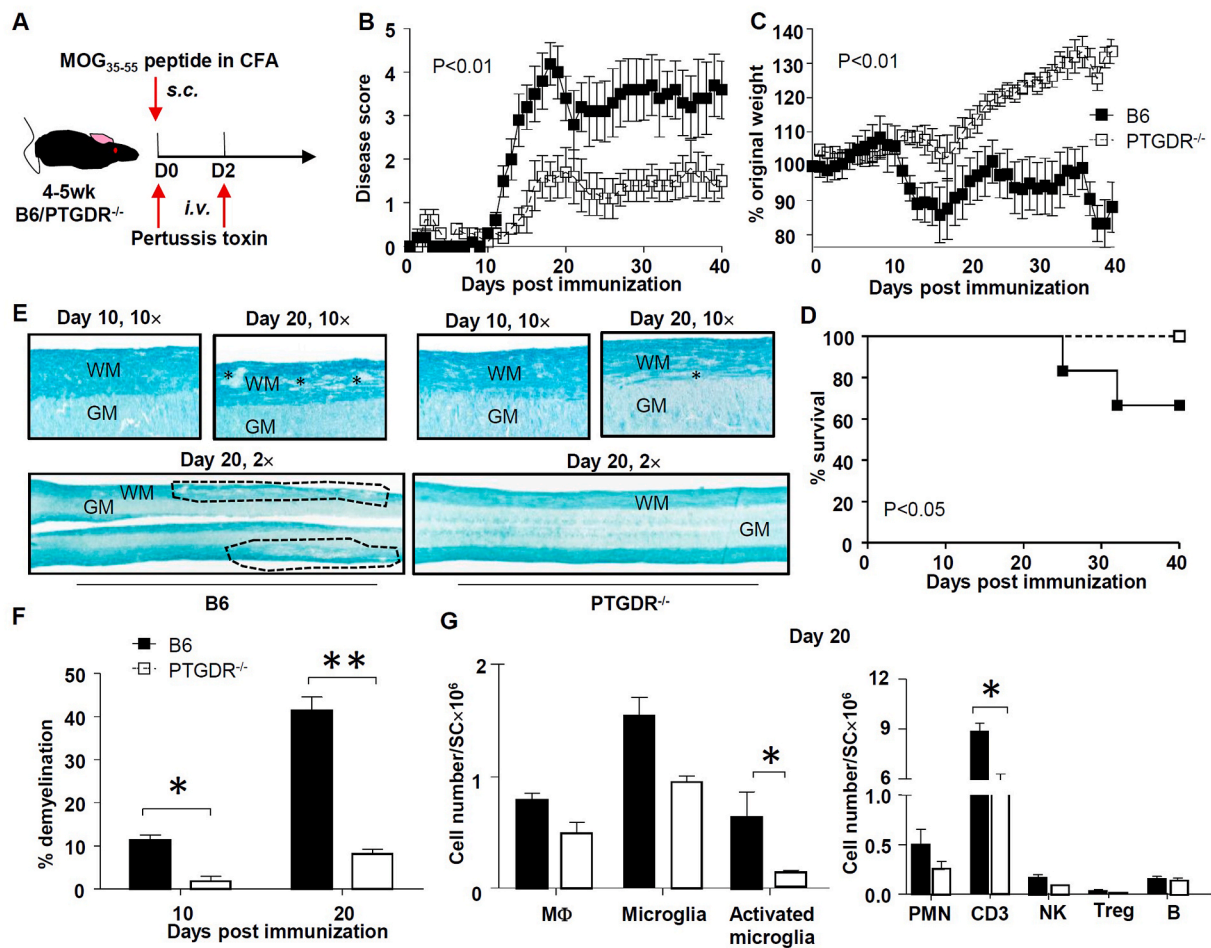


Fig. 1. PTGDR^{-/-} mice exhibit resistance to EAE induced by active immunization. (A) Protocol for immunization and EAE induction. (B) Disease score, (C) weight change and (D) survival of mice after immunization, n = 10. (E) Luxol fast blue staining of spinal cords of B6 and PTGDR^{-/-} mice on day 10 and 20 post immunization (lesions are labeled by * and dashed lines; WM: white matter, GM: grey matter). (F) Demyelination in spinal cords harvested on day 10 and 20 post immunization, n = 6–8. (G) Cell numbers of macrophage (MΦ, CD3⁻CD45^{hi}CD11b⁺CCR2⁺), microglia (CD3⁻CD45^{mid}CD11b⁺ CX3CR1⁺CCR2⁻), activated microglia (Iba-1⁺ microglia); and neutrophils (PMN, CD3⁻Ly6C⁺ Ly6G⁺), CD3 T cells, NK cells (CD3⁻ NK1.1⁺), Tregs (CD4⁺ Foxp3⁺) and B cells (CD3⁺ B220⁺) in spinal cords were determined by flow cytometry on day 20 post immunization, n = 4. (B–D, F and G) Data are shown as mean ± SEM and are representative of 3 independent experiments. *p < 0.05, **p < 0.01. (For interpretation of the references to color in this figure legend, the reader is referred to the Web version of this article.)

CD4 T cells reciprocally between B6 and PTGDR^{-/-} mice (Fig. 4A). Prior to transfer, CD4 T cells were exposed to cytokines to induce outgrowth of Th17 cells, as described in Methods. Adoptive transfer from immunized B6 mice induced progressive disease in B6 recipient mice, but only very mild clinical signs in PTGDR^{-/-} recipient mice (Fig. 4B). On the other hand, CD4 T cells from immunized PTGDR^{-/-} mice could not induce EAE in either B6 or PTGDR^{-/-} recipient mice. To track their distribution after transfer, donor CD4 T cells were labeled with carboxyfluorescein succinimidyl ester (CFSE) before adoptive transfer. As shown in Fig. 4C, CD4 T cells from PTGDR^{-/-} donor mice disappeared quickly in recipient mice and failed to migrate to the CNS, consistent with their pro-apoptotic phenotype (Fig. 3C). In contrast, CD4 T cells from donor B6 mice survived longer *in vivo* and infiltrated the CNS of B6 but not PTGDR^{-/-} recipients, indicating that the non-lymphocyte compartment/cells in PTGDR^{-/-} recipients failed to support the maintenance of donor T cells. Further supporting the conclusion that our results reflect a T cell-extrinsic effect, we found that T cells did not express PTGDR (Supplementary Figure 4A).

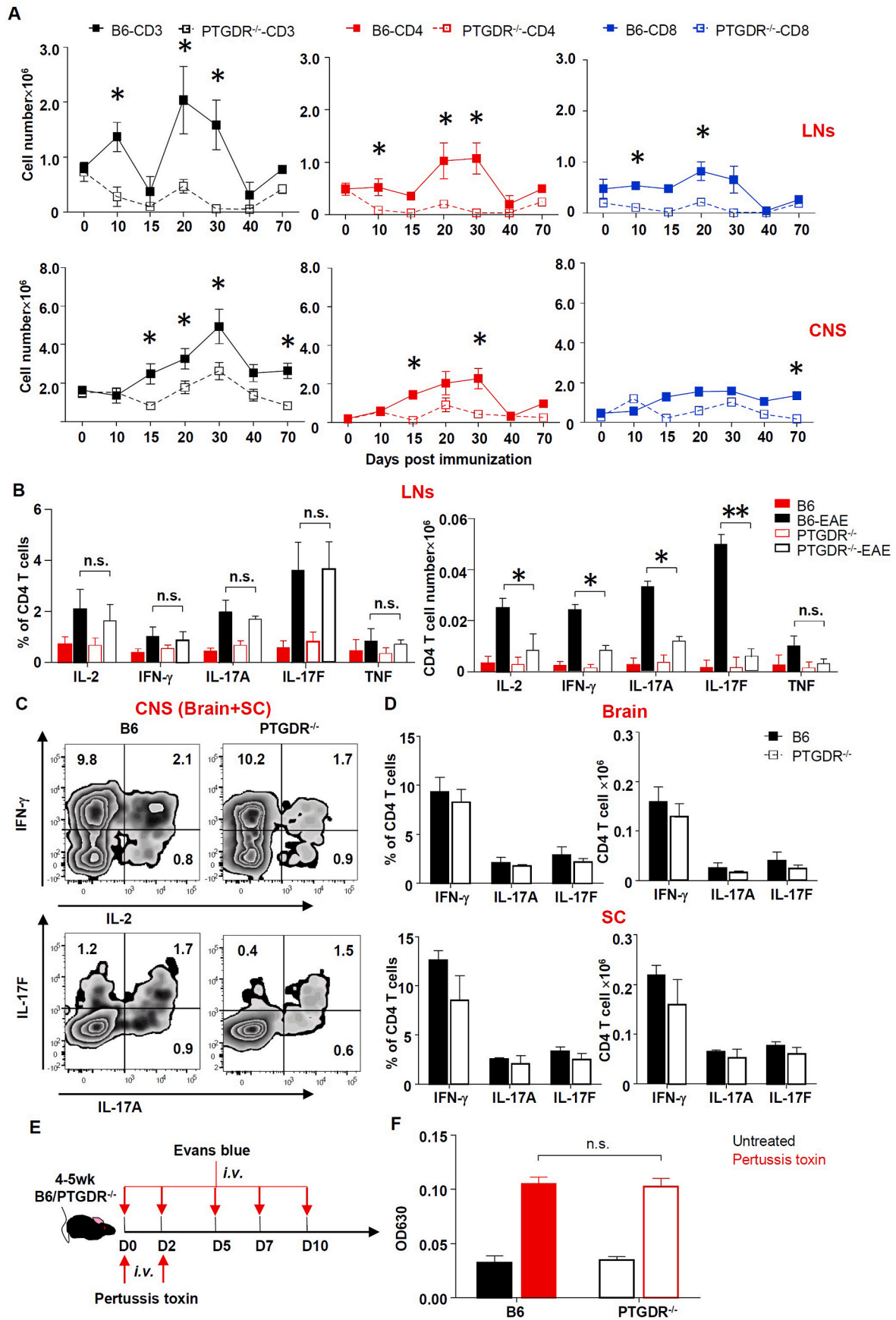
3.5. Conditional knock out of PTGDR in DCs reduced susceptibility to EAE

Since PTGDR is expressed primarily on myeloid cells

(Supplementary Figure 4), we next conditionally deleted PTGDR from myeloid cell subsets, using PTGDR^{lox} mice crossed to mice expressing Cre selectively in microglia (CX3CR1-Cre), monocytes/macrophages/granulocytes (LysM-Cre), or DCs (zDC-Cre) to generate CX3CR1, LysM or zDC conditional PTGDR knockout mice (CX3CR1-PTGDR^{-/-}, LysM-PTGDR^{-/-} and zDC-PTGDR^{-/-}) mice respectively (Fig. 5A and C). Although EAE onset was modestly delayed, CX3CR1-PTGDR^{-/-} and LysM-PTGDR^{-/-} mice developed EAE with severity similar to that of B6 mice (Fig. 5B and D). In marked contrast, zDC-PTGDR^{-/-} mice developed mild EAE, similar to that observed in PTGDR^{-/-} mice (Fig. 5E), accompanied by reduced CD4 T cell accumulation in the LNs and CNS (Fig. 5F).

3.6. PTGDR^{-/-} DCs ameliorate EAE by diminishing MOG₃₅₋₅₅-specific T cell response via enhanced PDL-1/PD-1 signaling

To confirm the role of PGD₂/PTGDR signaling on DCs in EAE induction, MOG₃₅₋₅₅ peptide-loaded DCs (MOG₃₅₋₅₅-DCs) from B6 and PTGDR^{-/-} mice were used to immunize mice of both strains (Fig. 6A). As expected, immunization with PTGDR^{-/-} DCs induced mild EAE in both B6 and PTGDR^{-/-} mice compared to B6 DC (Fig. 6B). Of note, disease was milder in PTGDR^{-/-} recipient mice. Generally, transferred



(caption on next page)

Fig. 2. Dynamics and function of T cells. (A) Dynamics of CD3, CD4 and CD8 T cell accumulation in LNs and CNS at indicated times post immunization, n = 5. (B-D) Percentage and cell number of cytokine (IL-2, IFN- γ , IL-17A, IL-17F and TNF)-expressing CD4 T cells from LNs (B) and brains, spinal cords (SC) (C and D) of mice harvested on day 10 post immunization, n = 8. Cells were stimulated with MOG₃₅₋₅₅ directly *ex vivo*. (E) Protocol for Evans blue assay. (F) OD reading at 630 nm of brain supernatants from Evans blue-treated mice, n = 4. (A, B, D and F) Data are shown as mean \pm SEM and are representative of 3 independent experiments. PT-pertussis toxin. *p < 0.05, **p < 0.01. (For interpretation of the references to color in this figure legend, the reader is referred to the Web version of this article.)

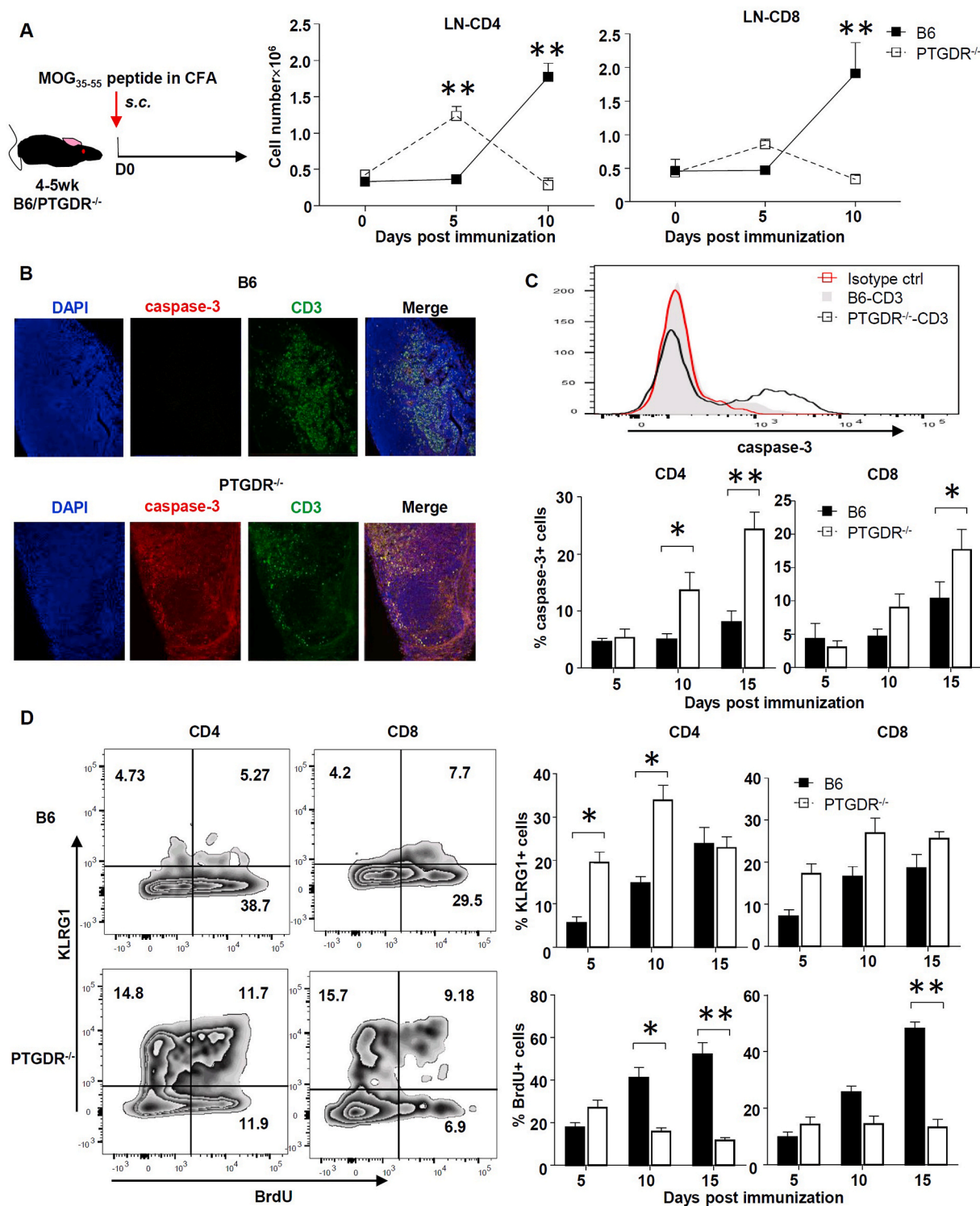


Fig. 3. Activation-induced apoptosis of T cells in LN of PTGDR^{-/-} mice at early times after immunization. (A) Dynamics of total CD4 and CD8 T cell numbers in LNs of mice, n = 5. (B) caspase-3⁺ CD3⁺ T cells in LNs of mice. (C) Expression of cleaved caspase-3 in LN CD4 and CD8 T cells determined by flow cytometry, n = 4. (D) Expression of KLRG1 and BrdU in LN CD4 and CD8 T cells harvested at indicated times post immunization, n = 4. Flow cytometric plot demonstrates KLRG1 and BrdU expression on day 10 post immunization. Data are shown as mean \pm SEM and are representative of 3 independent experiments. *p < 0.05, **p < 0.01.

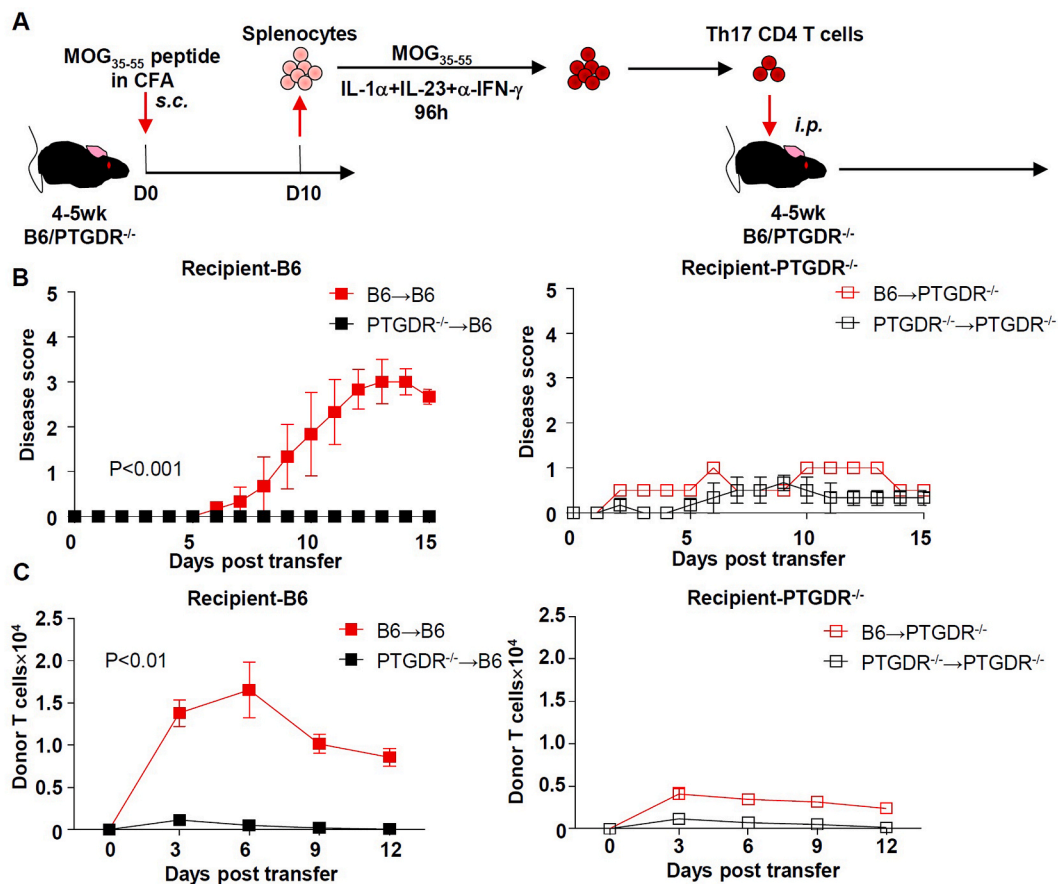


Fig. 4. PTGDR in recipient mice is required for development of EAE. (A) Protocol for generating Th17 CD4 T cells for adoptive transfer model. (B) Disease scores after adoptive transfer of B6 or PTGDR^{-/-} CD4 T cells into B6 or PTGDR^{-/-} recipients. (C) Dynamics of donor T cell accumulation in lymphoid tissues. (B and C) $n = 5$, data are shown as mean \pm SEM and are representative of 3 independent experiments. * $p < 0.05$.

DCs are undetectable after 48 h post injection [36] but peptide could be released for cross-presentation by DCs present in recipient mice. In this case, DCs in recipient PTGDR^{-/-} mice would be expected to induce attenuated EAE compared to those in B6 recipients. In addition to their ameliorating effects in EAE induction, administration of MOG₃₅₋₅₅-DCs from PTGDR^{-/-} mice after disease initiation (day 9, 12, and 15 post immunization, when T cells in B6 mice are in expansion as shown in Figs. 2A and 3A, D) also decreased the severity of EAE in B6 mice (Fig. 6J–K) and increased CD4 T cell apoptosis, indicating their therapeutic efficacy. These results strongly indicate that PD-1/PTGDR signaling on DCs is critical for the pathogenesis of EAE.

To determine the basis of increased CD4 T cell apoptosis, we measured levels of PD-L1 and PD-1 on DCs and T cells, respectively. Similar levels of PD-L1 were expressed on B6 and PTGDR^{-/-} DCs (Fig. 6C), but, in contrast, a higher percentage of CD4 T cells from LNs of immunized PTGDR^{-/-} mice expressed PD-1 (Fig. 6D and Supplementary Figure 5A). Treating *in vitro* co-cultures of CD11c cells and CD3 T cells (treated to induce Th17 CD4 T cells) (Supplementary Figure 5B) with anti-PD-1 antibody increased the numbers of total and MOG₃₅₋₅₅-specific IL-17F-secreting CD4 T cells but not CD8 T cells (Fig. 6E and Supplementary Figure 5C). *In vivo* treatment with anti-PD-1 antibody also reversed EAE attenuation in PTGDR^{-/-} mice (Fig. 6F and G). Augmented clinical disease was accompanied by decreased caspase-3 expression (Supplementary Figure 5D) and increased accumulation of total and MOG₃₅₋₅₅-specific CD4 T cells expressing IFN- γ and IL-17F after direct *ex vivo* stimulation) in both LNs and CNS of PTGDR^{-/-} mice (Fig. 6H and I). In contrast, blocking of another T cell apoptosis-related signaling pathway, Fas-FasL, increased total and MOG₃₅₋₅₅-specific T cell numbers *in vitro* but showed no role in diminished EAE severity in

PTGDR^{-/-} mice (Supplementary Fig. 5E–G). Together, these results indicate that decreased numbers of EAE antigen-specific CD4 T cells in the LNs and CNS correlated with PD-1 expression and probable T cell apoptosis.

3.7. Increased IL-1 β in PTGDR^{-/-} DCs contributes to EAE attenuation

To delineate changes in DC gene expression that contribute to attenuated EAE in PTGDR^{-/-} DCs, we purified DCs from the LNs of B6 and PTGDR^{-/-} mice and performed RNA sequencing and subsequent analyses of gene expression. The absence of PTGDR signaling resulted in differential expression of 20 genes, with a cutoff of twofold difference in expression (Fig. 7A). Pathway analyses demonstrated changes in several immune response pathways. In particular, expression of genes involved in antigen processing and presentation, which may contribute to over-activation of T cell during the early phase of EAE in PTGDR^{-/-} mice was increased (Fig. 7B). However, no differences were identified in expression of MHC-I, MHC-II or co-stimulatory molecules CD80, CD83, CD86 on DCs from B6 and PTGDR^{-/-} mice (Supplementary Figure 6). IFI208 (PYDC3), involved in suppressing inflammasome activation and IL-1 β expression [15], was prominently decreased in PTGDR^{-/-} DCs (Fig. 7A), resulting in increased IL-1 β expression in PTGDR^{-/-} DCs when assessed by mRNA and protein assays (Fig. 7C and D). IL-1 β receptor blockade with Anakinra, an IL-1R antagonist, significantly increased the severity of EAE in PTGDR^{-/-} mice and resulted in increased accumulation of total CD4 T cells in LNs and CNS (Fig. 7E–G). Notably, Anakinra treatment of B6 mice reduced EAE severity (Fig. 7F), in agreement with previous results [40]. Finally, using CRISPR-Cas9 methodology, we deleted PTGDR expression in

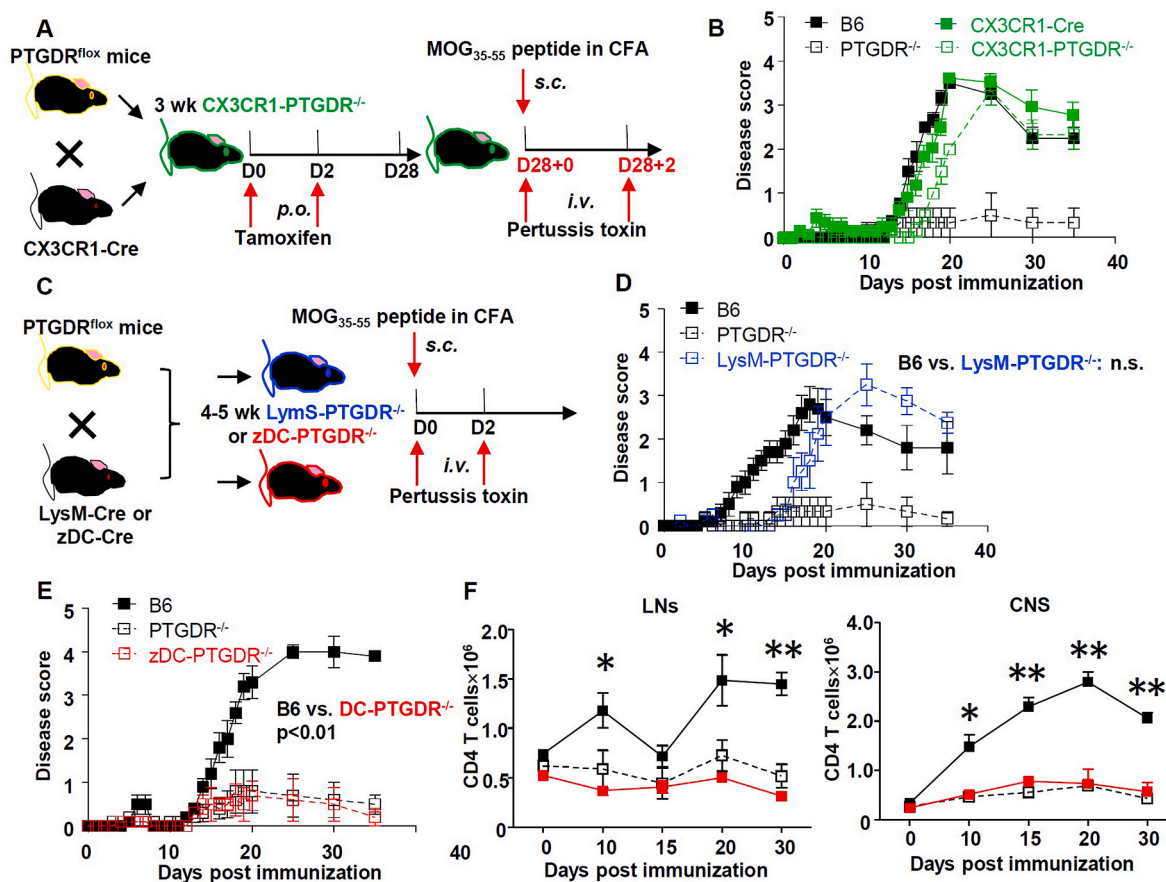


Fig. 5. Conditional deletion of PTGDR in DCs, but not CX3CR1⁺ or LysM⁺ cells reduced severity of EAE. (A, C) Protocol for EAE in CX3CR1-PTGDR^{-/-} mice (A), LysM- or zDC-PTGDR^{-/-} mice (C) and control mice. (B) Disease score of CX3CR1-PTGDR^{-/-} mice and control mice, n = 5. (D, E) Disease score of LysM- (D) and zDC- (E) PTGDR^{-/-} mice and control mice, n = 5. (F) Dynamics of total CD4 T cell numbers in LNs and CNS of zDC-PTGDR^{-/-} mice, n = 5. (B, D-F) Data are shown as mean ± SEM and are representative of 3 independent experiments. *p < 0.05, **p < 0.01.

human MDDCs (Fig. 7H and I). Compared to normal MDDCs, PTGDR^{-/-} MDDCs expressed higher levels of IL-1β after LPS stimulation, consistent with results obtained from PTGDR^{-/-} mice. Taken together, these data indicate that DC-derived IL-1β was critical for the amelioration of EAE in PTGDR^{-/-} mice by contributing to apoptosis of activated CD4 T cells.

4. Discussion

Here, we showed that the lack of signaling through the PGD₂ receptor, PTGDR, on DCs resulted in nearly complete amelioration of T-cell-mediated EAE. LNs (axillary, brachial and inguinal) are the major lymphoid sites for T cell priming and activation after immunization. At day 5 post immunization, PTGDR^{-/-} LNs were increased in cellularity compared to B6 LNs. However, by 10 day, LNs were smaller and the number of MOG₃₅₋₅₅-specific cells were much lower in PTGDR^{-/-} mice (Supplementary Figure 3A). This decrease reflected enhanced activation-induced apoptosis of T cells and subsequent decreased infiltration of peripheral leukocytes into the CNS and less activation of microglia (Figs. 1G, 2A and 3B-D), resulting in decreased EAE severity.

PGD₂/PTGDR signaling is considered anti-inflammatory [18–21]. In the absence of PGD₂/PTGDR signaling, expression of PYDC3, a protein which negatively regulates inflammasome activation [15], was decreased (Fig. 7A and C), resulting in increased IL-1β expression (Fig. 7D). PYDC3 has similarities to members of the human POP (Pyrin Only Proteins), which bind to members of the inflammasome pathway, inhibiting their function [41,42]. We previously showed that PGD₂ signaling through the PTGDR receptor is necessary for an optimal immune response after infection with a neurotropic coronavirus, murine

hepatitis virus (MHV). PTGDR^{-/-} mice succumbed to a normally non-lethal MHV infection, largely due to a decrease in PYDC3 and to increases in inflammasome activation and IL-1β expression [15]. In settings other than the brain, PGD₂/PTGDR signaling, while still anti-inflammatory, appears to have different effects. In the skin, PGD₂ expression results in delayed migration of Langerhans cells to LNs. *Schistosoma mansoni* has co-opted this pathway to delay the immune response after skin invasion, resulting in parasite persistence [19]. Similarly, in the lungs, age-related increases in PGD₂ resulted in delayed DC migration to LN, with resulting suboptimal T cell responses and increased mortality after infection with severe acute respiratory syndrome-coronavirus (SARS-CoV). Survival was improved after treatment with a PGD₂/PTGDR antagonist [16]. In addition to PGD₂, 15-deoxy-delta 12,14-prostaglandin J2 (15-PGJ₂), a PGD₂ downstream product, is another PTGDR ligand with a longer half-life *in vivo* [43,44]. Administration of 15-PGJ₂ ameliorated acute lung injury, whereas an absence of hematopoietic PGD synthase, required for PGD₂ and 15-PGJ₂ synthesis, resulted in disease enhancement [45]. The relative importance of PGD₂ and 15-PGJ₂ in PTGDR signaling may vary under different conditions, although this requires further evaluation.

Gene expression analyses of B6 and PTGDR^{-/-} DCs from MOG₃₅₋₅₅ peptide-immunized mice demonstrated changes in immune cell adhesion and inflammatory-related signal pathways (Fig. 7B). Most prominently, PYDC3 expression was decreased in PTGDR^{-/-} DCs, resulting in increased IL-1β expression. Consistent with a role for IL-1β in attenuated EAE, treatment with Anakinra resulted in the development of clinically evident EAE. However, IL-1β has variable effects in other models of EAE. Deletion of IL-1 receptor associated kinase (IRAK)-M was found to increase the severity of EAE by diminishing type 2

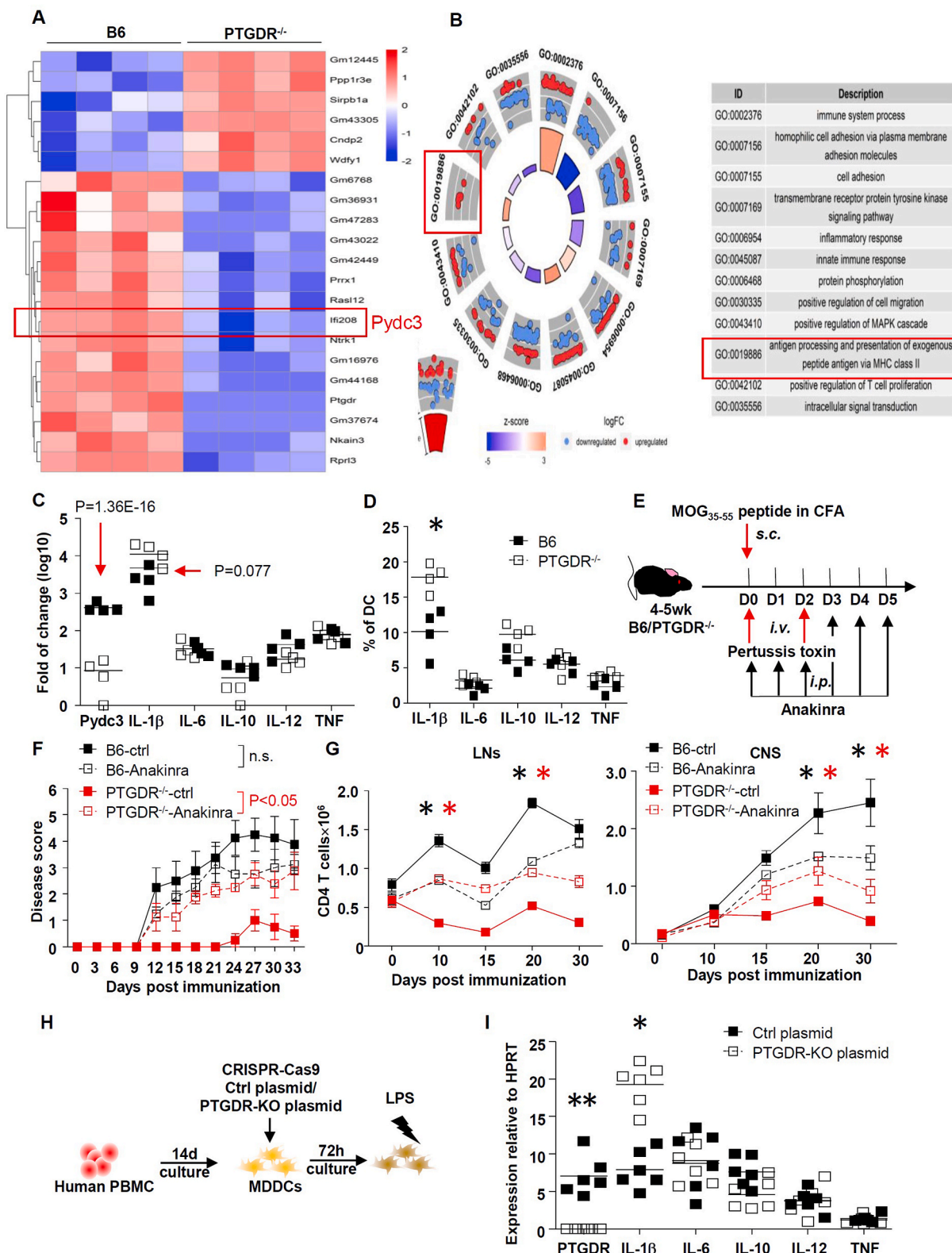


Fig. 7. Increased IL-1 β in PTGDR-deficient DCs contribute to resistance of PTGDR^{-/-} mice to EAE. (A-C) Gene expression assessed by NextSeq (A, C) and signal pathway (B) changes in DCs (harvested on day 6 post immunization), n = 4. (D) Cytokine expression (IL-1 β , IL-6, IL-10, IL-12, TNF) by DCs harvested from LNs on day 6 post immunization assessed by flow cytometry, n = 4. (E) Protocol for *in vivo* IL-1 β blockade after peptide immunization. (F) Disease score of immunized mice receiving anti-IL-1 β or isotype control, n = 5. (G) Dynamics of CD4 T cell accumulation in LNs and CNS harvested at indicated times post immunization, n = 5. *(black) differences between B6-ctrl and B6-anakinra groups. *(red) differences between PTGDR^{-/-}-ctrl and PTGDR^{-/-}-anakinra groups. (H) Protocol for engineering human PTGDR^{-/-} MDDCs, using CRISPR-Cas9, as described in Methods. Efficacy of deletion was monitored by PCR for each donor. (I) RNA expression of inflammation-related molecules (IL-1 β , IL-6, IL-10, IL-12, TNF) in LPS-treated and untreated MDDCs was determined by RT-PCR, n = 6. (C, D, F and G) Data are shown as mean \pm SEM and are representative of 3 independent experiments. *p < 0.05, **p < 0.01. (For interpretation of the references to color in this figure legend, the reader is referred to the Web version of this article.)

microglia polarization [46], whereas in other cases, blocking IL-1 β signaling resulted in diminished EAE [13,47]. Consistent with a pathogenic role for IL-1 β in B6 (PTGDR^{+/+}) mice with EAE, we found that Anakinra treatment resulted in a decrease in CD4 T cell accumulation, and, to a lesser extent, in clinical disease (Fig. 7F and G). Together, these results suggest that IL-1 β is required for optimal activation of autoreactive T cells in B6 mice; the augmented expression that occurs in the absence of PTGDR signaling results in activation-induced T cell apoptosis.

It is noteworthy that, although DCs appear to be the most important cellular source for IL-1 β in EAE, mast cells also express IL-1 β [33] and were recently identified as important effectors in pathogenesis of MS and EAE [33,48]. However, data obtained from MOG₃₅₋₅₅-immunized zDC-PTGDR^{-/-} mice (Fig. 5E) and from mice after MOG₃₅₋₅₅-DC immunization or treatment (Fig. 6B and K) indicated that DC effects were dominant in PTGDR^{-/-} mice, although effects may also be mediated by monocyte-derived DCs. Monocyte-derived macrophages are also critical for EAE development through expression of pro-inflammatory molecules essential for the development of neuroinflammation [1,49–51]. Microglia have dual roles in EAE, in enhancing and prolonging neuroinflammation [52,53], but also suppressing relapse in relapsing-remitting EAE by inhibiting the proliferation of CD4 T cells in the CNS [54]. The onset of EAE was delayed in CX3CR1-PTGDR^{-/-} and LysM-PTGDR^{-/-} mice suggesting that PTGDR signaling on microglia, or macrophages or neutrophils, respectively had a role in disease development, albeit a small one, because the severity of disease was similar to that observed in B6 mice (Fig. 5B, D).

We found that decreased T cell numbers observed in PTGDR^{-/-} mice was reversed by treatment with anti-PD-1 antibody (Fig. 6E). Both Fas/FasL and PD-1/PD-L1 interactions inhibit T cell activation and oligodendrocyte apoptosis in EAE [55]. Previous studies demonstrated a variable role for Fas/FasL in EAE, as FasL expressed on MBP-specific CD8 T cells was shown to promote ROS production in the brain and increase disease severity [8], whereas astrocyte-expressed FasL mediated autoimmune T cell elimination, contributing to recovery [56]. Although blocking either of these signaling pathways in PTGDR^{-/-} T cells improved survival in culture, only PD-1 blockade increased the susceptibility of PTGDR^{-/-} mice to EAE (Fig. 6G–I and Supplementary Figure 5G). This difference might result from the increased expression of PD-1 but not Fas on activated CD4 T cells in PTGDR^{-/-} mice (Fig. 6D and Supplementary Figure 5E).

5. Conclusions

In summary, we demonstrate a critical role for PGD₂/PTGDR signaling in DCs in preventing apoptosis of autoimmune T cells in EAE. We also demonstrate that while IL-1 β has pathogenic effects in wild type mice with EAE, it is, paradoxically, protective at higher levels as occurs in PTGDR^{-/-} mice. These results suggest that targeting PGD₂/PTGDR signaling is a potential strategy for preventing or even treating neuroinflammation by enhancing T cell apoptosis, thereby diminishing autoimmune T cell responses.

Author contributions

J.Z. and S.P., initiated and designed the study. J. Z., and A. S. performed experiments and collected data. J. Z., D. M., Q. Z., J. L. and S. P. analyzed data. J. Z., S. P. wrote the initial manuscript. S.N. provided a critical reagent. All authors contributed to writing and revising the manuscript and have seen and approved the final version.

Declaration of competing interest

The authors have declared that no conflicts of interest exist.

Acknowledgements

Supported in part by grants from the NIH (RO1 NS36592) and National Multiple Sclerosis Society (RG 5340-A-7).

Appendix A. Supplementary data

Supplementary data to this article can be found online at <https://doi.org/10.1016/j.jaut.2020.102508>.

References

- [1] J. Goverman, Autoimmune T cell responses in the central nervous system, *Nat. Rev. Immunol.* (9) (2009) 393–407.
- [2] V.K. Tuohy, M. Yu, L. Yin, J.A. Kawczak, R.P. Kinkel, Spontaneous regression of primary autoreactivity during chronic progression of experimental autoimmune encephalomyelitis and multiple sclerosis, *J. Exp. Med.* 189 (1999) 1033–1042.
- [3] T. Ziemssen, F. Ziemssen, The role of the humoral immune system in multiple sclerosis (MS) and its animal model experimental autoimmune encephalomyelitis (EAE), *Autoimmun. Rev.* (4) (2005) 460–467.
- [4] P.K. Stys, S. Tsutsui, Recent advances in understanding multiple sclerosis, *Fl000Res* (8) (2019).
- [5] H. Lassmann, The changing concepts in the neuropathology of acquired demyelinating central nervous system disorders, *Curr. Opin. Neurol.* (32) (2019) 313–319.
- [6] S.B. Simmons, E.R. Pierson, S.Y. Lee, J.M. Goverman, Modeling the heterogeneity of multiple sclerosis in animals, *Trends Immunol.* 34 (2013) 410–422.
- [7] L. Van Kaer, J.L. Postoak, C. Wang, G. Yang, L. Wu, Innate, innate-like and adaptive lymphocytes in the pathogenesis of MS and EAE, *Cell. Mol. Immunol.* (16) (2019) 531–539.
- [8] C.A. Wagner, P.J. Roque, T.R. Mileur, D. Liggitt, J.M. Goverman, Myelin-specific CD8+ T cells exacerbate brain inflammation in CNS autoimmunity, *J. Clin. Invest.* 130 (2019) 203–213.
- [9] F. Coutant, P. Miossec, Altered dendritic cell functions in autoimmune diseases: distinct and overlapping profiles, *Nat. Rev. Rheumatol.* 12 (2016) 703–715.
- [10] A. Schlitzer, F. Ginhoux, Organization of the mouse and human DC network, *Curr. Opin. Immunol.* (26) (2014) 90–99.
- [11] C. Sie, T. Korn, Dendritic cells in central nervous system autoimmunity, *Semin. Immunopathol.* 39 (2017) 99–111.
- [12] B. Ajami, N. Samusik, P. Wiegand, P.P. Ho, A. Crotti, Z. Bjornson, et al., Single-cell mass cytometry reveals distinct populations of brain myeloid cells in mouse neuroinflammation and neurodegeneration models, *Nat. Neurosci.* 21 (2018) 541–551.
- [13] C.C. Lin, B.T. Edelson, New insights into the role of IL-1 β in experimental autoimmune encephalomyelitis and multiple sclerosis, *J. Immunol.* 198 (2017) 4553–4560.
- [14] D. Sagar, N.P. Singh, R. Ginwala, X. Huang, R. Philip, M. Nagarkatti, et al., Antibody blockade of CLEC12A delays EAE onset and attenuates disease severity by impairing myeloid cell CNS infiltration and restoring positive immunity, *Sci. Rep.* 7 (2017) 2707.
- [15] R. Vijay, A.R. Fehr, A.M. Janowski, J. Athmer, D.L. Wheeler, M. Grunewald, et al., Virus-induced inflammasome activation is suppressed by prostaglandin D₂/DP1 signaling, *Proc. Natl. Acad. Sci. U. S. A.* 114 (2017) E5444–E5453.
- [16] J. Zhao, J. Zhao, K. Legge, S. Perlman, Age-related increases in PGD(2) expression impair respiratory DC migration, resulting in diminished T cell responses upon respiratory virus infection in mice, *J. Clin. Invest.* 121 (2011) 4921–4930.
- [17] S. Narumiya, T. Ogorochi, K. Nakao, O. Hayaishi, Prostaglandin D₂ in rat brain, spinal cord and pituitary: basal level and regional distribution, *Life Sci.* 31 (1982) 2093–2103.
- [18] N. Gualde, H. Harizi, Prostanoids and their receptors that modulate dendritic cell-mediated immunity, *Immunol. Cell Biol.* (82) (2004) 353–360.
- [19] V. Angeli, C. Faveeuw, O. Roye, J. Fontaine, E. Teissier, A. Capron, et al., Role of the parasite-derived prostaglandin D₂ in the inhibition of epidermal Langerhans cell migration during schistosomiasis infection, *J. Exp. Med.* 193 (2001) 1135–1147.
- [20] M. Herve, V. Angeli, E. Pinzar, R. Wintjens, C. Faveeuw, S. Narumiya, et al., Pivotal roles of the parasite PGD₂ synthase and of the host D prostanoid receptor 1 in schistosome immune evasion, *Eur. J. Immunol.* 33 (2003) 2764–2772.
- [21] Y. Ouhaddi, S.S. Nebbaki, L. Habouri, H. Afif, B. Lussier, M. Kapoor, et al., Deletion of the prostaglandin D₂ receptor DP1 exacerbates aging-associated and instability-induced osteoarthritis, *Arthritis Rheum.* 69 (2017) 1784–1795.
- [22] N. Kim, A.D. Luster, Regulation of immune cells by eicosanoid receptors, *Sci. World J.* (7) (2007) 1307–1328.
- [23] K. Tanaka, H. Hirai, S. Takano, M. Nakamura, K. Nagata, Effects of prostaglandin D₂ on helper T cell functions, *Biochem. Biophys. Res. Commun.* 316 (2004) 1009–1014.
- [24] K. Kabashima, S. Narumiya, The DP receptor, allergic inflammation and asthma, *Prostaglandins Leukot. Essent. Fatty Acids* 69 (2003) 187–194.
- [25] P. Gosset, F. Bureau, V. Angeli, M. Pichavant, C. Faveeuw, A.B. Tonnel, et al., Prostaglandin D₂ affects the maturation of human monocyte-derived dendritic cells: consequence on the polarization of naive Th cells, *J. Immunol.* 170 (2003) 4943–4952.
- [26] F.G. Gervais, R.P. Cruz, A. Chateaufneuf, S. Gale, N. Sawyer, F. Nantel, et al., Selective modulation of chemokinesis, degranulation, and apoptosis in eosinophils through the PGD₂ receptors CRTH2 and DP, *J. Allergy Clin. Immunol.* 108 (2001)

- 982–988.
- [27] A.S. Ahmad, M. Ahmad, T. Maruyama, S. Narumiya, S. Dore, Prostaglandin D2 DP1 receptor is beneficial in ischemic stroke and in acute excitotoxicity in young and old mice, *Age* (32) (2010) 271–282.
- [28] X. Liang, L. Wu, T. Hand, K. Andreasson, Prostaglandin D2 mediates neuronal protection via the DP1 receptor, *J. Neurochem.* (92) (2005) 477–486.
- [29] I. Mohri, K. Kadoyama, T. Kanekiyo, Y. Sato, K. Kagitani-Shimono, Y. Saito, et al., Hematopoietic prostaglandin D synthase and DP1 receptor are selectively upregulated in microglia and astrocytes within senile plaques from human patients and in a mouse model of Alzheimer disease, *J. Neuropathol. Exp. Neurol.* 66 (2007) 469–480.
- [30] I. Mohri, M. Taniike, H. Taniguchi, T. Kanekiyo, K. Aritake, T. Inui, et al., Prostaglandin D2-mediated microglia/astrocyte interaction enhances astrogliosis and demyelination in twitcher, *J. Neurosci.* (26) (2006) 4383–4393.
- [31] S. Saleem, H. Zhuang, A.J. de Brum-Fernandes, T. Maruyama, S. Narumiya, S. Dore, PGD(2) DP1 receptor protects brain from ischemia-reperfusion injury, *Eur. J. Neurosci.* (26) (2007) 73–78.
- [32] N. Sawyer, E. Cauchon, A. Chateaufneuf, R.P. Cruz, D.W. Nicholson, K.M. Metters, et al., Molecular pharmacology of the human prostaglandin D2 receptor, CRTH2. *Br J Pharmacol.* 137 (2002) 1163–1172.
- [33] A.E. Russi, M.E. Walker-Caulfield, M.A. Brown, Mast cell inflammasome activity in the meninges regulates EAE disease severity, *Clin. Immunol.* 189 (2018) 14–22.
- [34] V.P. Badovinac, K.A. Messingham, A. Jabbari, J.S. Haring, J.T. Harty, Accelerated CD8+ T-cell memory and prime-boost response after dendritic-cell vaccination, *Nat. Med.* 11 (2005) 748–56.
- [35] D. Burger, N. Molnarfi, M.S. Weber, K.J. Brandt, M. Benkhoucha, L. Gruaz, et al., Glatiramer acetate increases IL-1 receptor antagonist but decreases T cell-induced IL-1beta in human monocytes and multiple sclerosis, *Proc. Natl. Acad. Sci. U. S. A.* 106 (2009) 4355–4359.
- [36] R.L. Brunette, J.M. Young, D.G. Whitley, I.E. Brodsky, H.S. Malik, D.B. Stetson, Extensive evolutionary and functional diversity among mammalian AIM2-like receptors, *J. Exp. Med.* 209 (2012) 1969–1983.
- [37] L. de Almeida, S. Khare, A.V. Misharin, R. Patel, R.A. Ratsimandresy, M.C. Wallin, et al., The PYRIN domain-only protein POP1 inhibits inflammasome assembly and ameliorates inflammatory disease, *Immunity* 43 (2015) 264–276.
- [38] N.K. Maier, S.H. Leppa, M. Moayeri, The cyclopentenone prostaglandin 15d-PGJ2 inhibits the NLRP1 and NLRP3 inflammasomes, *J. Immunol.* 194 (2015) 2776–2785.
- [39] D.S. Straus, G. Pascual, M. Li, J.S. Welch, M. Ricote, C.H. Hsiang, et al., 15-deoxy-delta 12,14-prostaglandin J2 inhibits multiple steps in the NF-kappa B signaling pathway, *Proc. Natl. Acad. Sci. U. S. A.* 97 (2000) 4844–4849.
- [40] T. Murata, K. Aritake, Y. Tsubosaka, T. Maruyama, T. Nakagawa, M. Hori, et al., Anti-inflammatory role of PGD2 in acute lung inflammation and therapeutic application of its signal enhancement, *Proc. Natl. Acad. Sci. U. S. A.* 110 (2013) 5205–5210.
- [41] B. Liu, Y. Gu, S. Pei, Y. Peng, J. Chen, L.V. Pham, et al., Interleukin-1 receptor associated kinase (IRAK)-M-mediated type 2 microglia polarization ameliorates the severity of experimental autoimmune encephalomyelitis (EAE), *J. Autoimmun.* 102 (2019) 77–88.
- [42] S.M. Allan, P.J. Tyrrell, N.J. Rothwell, Interleukin-1 and neuronal injury, *Nat. Rev. Immunol.* (5) (2005) 629–640.
- [43] D. Elieh-Ali-Komi, Y. Cao, Role of mast cells in the pathogenesis of multiple sclerosis and experimental autoimmune encephalomyelitis, *Clin. Rev. Allergy Immunol.* 52 (2017) 436–445.
- [44] S.S. Duffy, J.G. Lees, G. Moalem-Taylor, The contribution of immune and glial cell types in experimental autoimmune encephalomyelitis and multiple sclerosis, *Mult Scler Int* 2014 (2014) 285245.
- [45] S. Li, Y. Wu, D. Yang, C. Wu, C. Ma, X. Liu, et al., Gasdermin D in peripheral myeloid cells drives neuroinflammation in experimental autoimmune encephalomyelitis, *J. Exp. Med.* 216 (2019) 2562–2581.
- [46] R. Yamasaki, H. Lu, O. Butovsky, N. Ohno, A.M. Rietsch, R. Cialic, et al., Differential roles of microglia and monocytes in the inflamed central nervous system, *J. Exp. Med.* 211 (2014) 1533–1549.
- [47] E.M. Chastain, D.S. Duncan, J.M. Rodgers, S.D. Miller, The role of antigen presenting cells in multiple sclerosis, *Biochim. Biophys. Acta* 1812 (2011) 265–274.
- [48] A. Shemer, S. Jung, Differential roles of resident microglia and infiltrating monocytes in murine CNS autoimmunity, *Semin. Immunopathol.* 37 (2015) 613–623.
- [49] S. Tanabe, S. Saitoh, H. Miyajima, T. Itokazu, T. Yamashita, Microglia suppress the secondary progression of autoimmune encephalomyelitis, *Glia* 67 (2019) 1694–1704.
- [50] N. Hovelmeyer, Z. Hao, K. Kranidioti, G. Kassiotis, T. Buch, F. Frommer, et al., Apoptosis of oligodendrocytes via Fas and TNF-R1 is a key event in the induction of experimental autoimmune encephalomyelitis, *J. Immunol.* 175 (2005) 5875–5884.
- [51] X. Wang, F. Haroon, S. Karray, D. Martina, D. Schluter, Astrocytic Fas ligand expression is required to induce T-cell apoptosis and recovery from experimental autoimmune encephalomyelitis, *Eur. J. Immunol.* 43 (2013) 115–124.
- [52] T. Matsuoka, M. Hirata, H. Tanaka, Y. Takahashi, T. Murata, K. Kabashima, et al., Prostaglandin D2 as a mediator of allergic asthma, *Science* 287 (2000) 2013–2017.
- [53] S. Mi, B. Hu, K. Hahm, Y. Luo, E.S. Kam Hui, Q. Yuan, et al., LINGO-1 antagonist promotes spinal cord remyelination and axonal integrity in MOG-induced experimental autoimmune encephalomyelitis, *Nat. Med.* 13 (2007) 1228–1233.
- [54] P. Rao, B.M. Segal, Experimental autoimmune encephalomyelitis, *Methods Mol. Biol.* 900 (2012) 363–380.
- [55] L. Baert, M. Benkhoucha, N. Popa, M.C. Ahmed, B. Manfroi, J. Boutonnat, et al., APRIL-mediated anti-inflammatory response of astrocytes in multiple sclerosis, *Ann. Neurol.* (85) (2019) 406–420.
- [56] L. Pewe, H. Zhou, J. Netland, C. Tangudu, H. Olivares, L. Shi, et al., A severe acute respiratory syndrome-associated coronavirus-specific protein enhances virulence of an attenuated murine coronavirus, *J. Virol.* 79 (2005) 11335–11342.